small NANO MICRO

Micropatterning

Ultrafast Large-Area Micropattern Generation in Nonabsorbing Polymer Thin Films by Pulsed Laser Diffraction

Ankur Verma, Ashutosh Sharma, and Giridhar U. Kulkarni*

An ultrafast, parallel, and beyond-the-master micropatterning technique for ultrathin (30–400 nm) nonabsorbing polymer films by diffraction of laser light through a 2D periodic aperture is reported. The redistribution of laser energy absorbed by the substrate causes self-organization of polymer thin films in the form of wrinklelike surface relief structures caused by localized melting and freezing of the thin film. Unlike conventional laser ablation and laser writing processes, low laser fluence is employed to only passively swell the polymer as a pre-ablative process without loss of material, and without absorption/reaction with incident radiation. Self-organization in the thin polymer film, aided by the diffraction pattern, produces microstructures made up of thin raised lines. These regular microstructures have far more complex morphologies than the mask geometry and very narrow line widths that can be an order of magnitude smaller than the openings in the mask. The microstructure morphology is easily modulated by changing the film thickness, aperture size, and geometry, and by changing the diffraction pattern.

1. Introduction

Micropattern generation[1,2] by multistep top-down techniques such as photolithography[3] and by the self-organization based methods such as controlled dewetting,[4,5] electric field lithography,[6] etc., produce a pattern morphology and pattern length scale commensurate with the mask, template, or master employed. We present here an ultra-fast, single-step technique of beyond-the-mask pattern generation in nonabsorbing thin (<500 nm) polymer films by harnessing the self-organization induced by the low-fluence laser diffraction patterns. In contrast to the nature of patterns generated by other techniques, the micropatterns obtained here by simple masks are in the form of complex lattice structures with line widths that can be tuned by the film thickness and can be more than an order of magnitude smaller than the mask openings.

The fabrication of patterned and functionalized polymeric surfaces is an area of increasing interest because of potential applications in microfluidics, microelectromechanical systems, polymer electronics, multifunctional coatings, and bioengineering.[1] In addition, patterned polymeric surfaces provide an inexpensive route to pattern other kinds of surfaces such as metals and ceramics.[2] Various lithography techniques are used to produce surface structures on polymer films and substrates.[3] The most widely used UV lithography requires light-sensitive polymers (photoresists) and involves multistep fabrication protocols (mask design, exposure, pattern developing, etc.). Lithography techniques produce the pattern geometry, pattern length scales and line widths that are commensurate with the mask openings.

There are also several techniques based on self-organization in soft materials for the generation of controlled micropatterns that can be contrasted with the thermal-energy-induced self-organization studied here. For example,

A. Verma, Prof. A. Sharma
Department of Chemical Engineering and DST Unit on Nanoscience
Indian Institute of Technology Kanpur
Kanpur, 208016, India
E-mail: ashutos@iitk.ac.in
Prof. G. U. Kulkarni
Chemistry and Physics of Materials Unit and DST Unit on Nanoscience
Jawaharlal Nehru Centre for Advanced Scientific Research
Bangalore, 560 064, India

DOI: 10.1002/smll.201001939

controlled dewetting of ultrathin (<100 nm) polymer films have been extensively studied as a promising tool for polymer patterning. Polymer thin films on physicochemically patterned substrates produce patterned arrays of polymer droplets when destabilized by either heating above their glass transition temperature (T_g) or by exposure to solvent vapor.[4] The characteristic length scales (feature size and wavelength) of dewetting strongly depend on the initial thickness of a polymer film.[5] The time scales involved in dewetting highly viscous polymer films are typically on the order of several minutes, and the structures can be aligned on the scale of physicochemically patterned templates used as substrates for dewetting. Other approaches for the self-organized patterning of thin films involve spatially varying patterned destabilizing force fields such as electric fields and adhesive forces, etc.[6]

A different strategy for polymer patterning involves the formation of surface relief structures in the form of wrinkling and buckling of the polymer films under the mechanical stresses generated during stretching-compression, rapid heating-cooling cycles, differential swelling-shrinkage etc.[7] The characteristic length scales of the wrinkling and buckling scales with film thickness and the stresses in the film and substrate.[8]

Another widely studied technique for the patterning of laser-absorbing polymers and other hard materials like metals, glass, and ceramics is laser ablation.[9] Depending on its absorption and interaction with the material, laser light may break the atomic bonds or cause material melting and removal or modify it chemically or physically. Use of pulsed lasers (nano-, pico-, or femtosecond) further adds the advantage of increased throughput by making it a continuous fabrication process. One can also use the structured light by incorporating interference and diffraction effects to produce more complex structures.[10,11] Under low laser fluence, swelling or material expansion has been observed as a pre-ablative process, which forms wrinklelike patterns on the surface.[12] However, a low absorption coefficient of the polymers (e.g., poor absorption of 355 nm laser in polystyrene (PS) and polymethylmethacrylate (PMMA)[13]) renders melting and subsequent pattern formation difficult unless some polymer-specific modifications are made for enhanced optical absorption.[14]

The current work presents the self-organized patterns generated by laser processing of thin (<400 nm) nonabsorbing polymer films coated on absorbing substrates. In this technique, the structured light resulting from the near-field diffraction from a small periodic aperture was employed on a thin polymer film coated on silicon. The third harmonic of a Nd-YAG laser (355 nm) was used as the incident radiation. A single pulse of the laser was sufficient to produce relief structures on the large areas of polymer thin films without any loss of material from the surface, making it a high-throughput, continuous process. The use of ultrathin polymeric films offers greater flexibility in controlling surface structures via self-organization.[6,7] Local melting caused by the absorption of structured light and rapid diffusion of heat in the substrate produce simple to complex structures that can be tuned by changing aperture size and geometry, polymer film thickness, and aperture substrate distance. This method is capable of producing ultrafast (≈100 ns), cheap, and large-area patterns (~cm^2) on a variety of polymers as it demands no special optical or chemical properties of the polymer. The patterns thus generated have some interesting and unique characteristics that are clearly differentiated from the patterns formed by other lithography- and self-organization-based methods: 1) the patterns are in the form of an open latticework structure consisting of fine lines with line-widths one to two orders of magnitude smaller than the mask openings; 2) the pattern geometry is far more complex than the mask geometry; 3) both the pattern length scales and morphology can be modulated by changing the film thickness.

2. Results and Discussion

Polymer thin films coated on different substrates were irradiated by a single pulse of a Nd-YAG laser and the patterns that evolved on the surface of polymer were examined under microscope. **Figure 1** shows a schematic of the experimental setup, highlighting different aperture geometries and the process variables. Effects of various process parameters, e.g., aperture size (a) and distance (l), film thickness, substrate, etc., on the evolution of patterns are investigated.

Different types of substrates such as silicon, quartz, glass, and ITO-coated glass were used for coating polymer thin films. With silicon as the substrate for polymeric films the patterns appeared prominently, whereas there were no patterns on the polymer films coated on glass and quartz. Polymer films on ITO-coated glass showed some poorly formed patterns. Based on these observations, it is evident that the substrate plays an important role in the proposed method of pattern formation in thin polymer films. For both the polymers (PS and PMMA), the absence of any pattern when coated on glass and quartz substrates is due to their transparency to 355 nm light.[13] Silicon, on the other hand, absorbs the radiation energy from the laser pulse and transfers it to the polymer in the form of thermal energy. The local heating and subsequent freezing cause reorganization of the polymer film in the form of wrinklelike surface relief patterns. The laser fluence used in these experiments was not sufficient to cause melting of silicon, which was confirmed by examining the substrate after

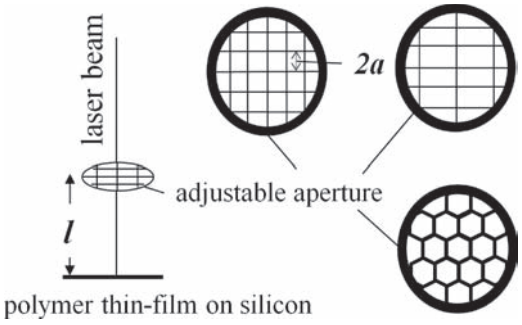

Figure 1. Schematic of the experimental setup, showing adjustable apertures of various types (square, rectangular, hexagonal openings). The distance between film and aperture (l) is adjusted by a micromanipulator.

small NANO MICRO

selective removal of the patterned polymer film. In the subsequent discussion silicon is used as the substrate for the patterning of polymer thin films.

We first investigated the effect of the laser beam on the polymer film without using any microaperture. Randomly distributed wrinklelike surface relief patterns appeared on the films of both PS and PMMA. There are two characteristic length scales of these patterns: wrinkle line width (w_c) and the mean separation between the wrinkle lines (L_c). Both of these are found to increase linearly with film thickness (**Figure 2**). Relatively thick films (100 nm < h < 400 nm) showed well developed, smooth, but sparse patterns. As the thickness is decreased, the patterns become increasingly denser and more fragmented. The line-width of ridges decreased linearly with the film thickness. Figure 2a shows the linear dependence of the mean interline distance between the wrinkles, L_c, on the film thickness in the case of both the PS and PMMA thin films. This linear dependence is in qualitative agreement with earlier work on the dependence of wrinkle wavelengths on PS films subjected to thermal and mechanical stresses.[8] Based on the refractive index of silicon at 355 nm, the surface reflection loss can be calculated, which is 75.77% at normal incident angle.[15] Further, simple calculations of heat transfer at room temperature showed that the heat conduction through the silicon wafer is extremely fast (within a few hundred nanoseconds). The thermal diffusivity of PS being three orders of magnitude less (Si: 0.91 $cm^2\ s^{-1}$, PS: $5.86 \times 10^{-4}\ cm^2\ s^{-1}$), one may expect compressive stresses in the polymer film leading to the formation of ridges on its surface. Use of thin nonabsorbing polymer films is an essential factor in this patterning technique, because the film should be thin enough to melt and reorganize before the heat diffuses away to the bulk of the conducting substrate. For the laser energies used in these experiments, films up to ≈400 nm could be patterned. Variation of the characteristic length-scales of the surface relief structures (Figure 2) is useful for optimizing the film thickness for a given diffraction pattern. For example, films thinner than 75 nm are required if a pattern with features of ≈10 μm is to be fabricated.

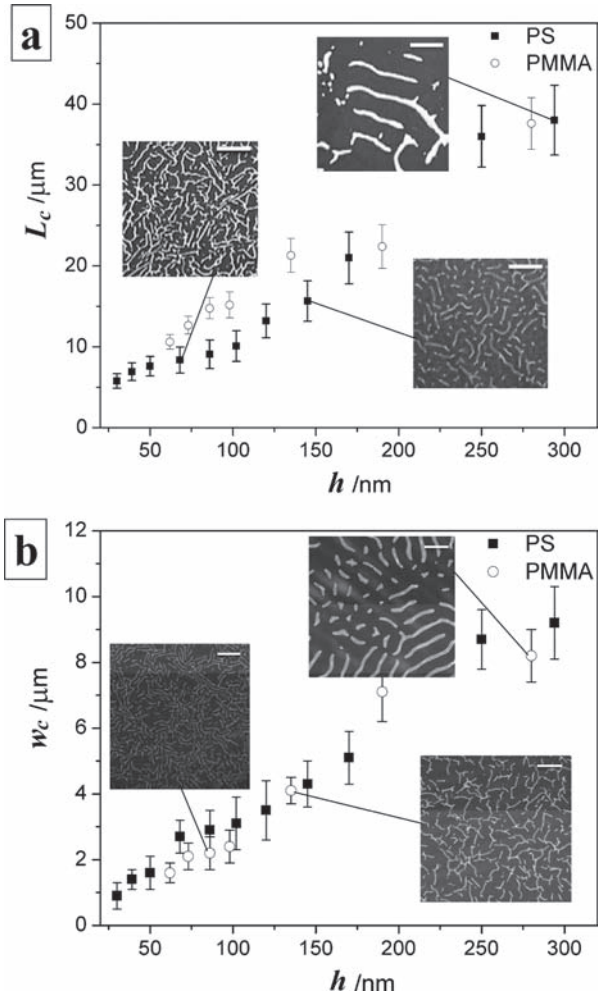

Figure 2. Wrinkle patterns formed on PS and PMMA thin films by exposure to a single laser pulse without any mask, and the dependence of characteristic length-scales of the pattern on the polymer film thickness. a) Mean separation of wrinkles, L_c, as a function of film thickness, h, shows linear dependence for both PS and PMMA. Insets show the optical micrographs of wrinkled PS films of thicknesses 68, 145, and 294 nm. b) Wrinkle line-width, w_c, as a function of film thickness shows a linear dependence for both PS and PMMA. Insets show the optical micrographs of the wrinkled PMMA films of thicknesses 86, 135, and 280 nm. (Scale bar: 50 μm)

Material properties such as molecular weight and thermal conductivity are some of the factors that govern L_c and w_c. To decrease L_c and w_c, lower molecular weight and higher thermal conductivity are desired, which will be investigated in future studies.

Next, we characterize the pattern modification and control by the use of diffraction gratings. The near-field diffraction is characterized by the Fresnel Number, F, defined as

$$F = a^2/\lambda l \quad (1)$$

where a is half aperture width, l is distance of the aperture from the substrate, and λ is the wavelength of incident light. Solving near-field diffraction equations for a square aperture, one can get the intensity distribution on the screen, shown in **Figure 3**.[16] These patterns depend only on F, but not on the aperture width or screen distance individually. Some of the notable features in these patterns are: the maxima adjacent to the edges of the square are most prominent; the number of intermediate maxima increase with F; the difference in intensity at bright and dark regions reduces with increasing F; the center appears bright in the case of odd numbered values of F. The patterns formed by a square aperture can be thought of as an orthogonal overlap of two identical single slits. By the same argument, one can constitute the near-field diffraction patterns of hexagonal aperture as the combination of three identical single slits placed at a 60° angle to each other (simulations for hexagonal as well as rectangular apertures are not shown here).

In the present work, apertures of different sizes and geometries have been used to establish a better understanding of the effects of the diffraction pattern on the relief structures generated on thin polymer films. Results for four different types of apertures are reported here: square apertures with

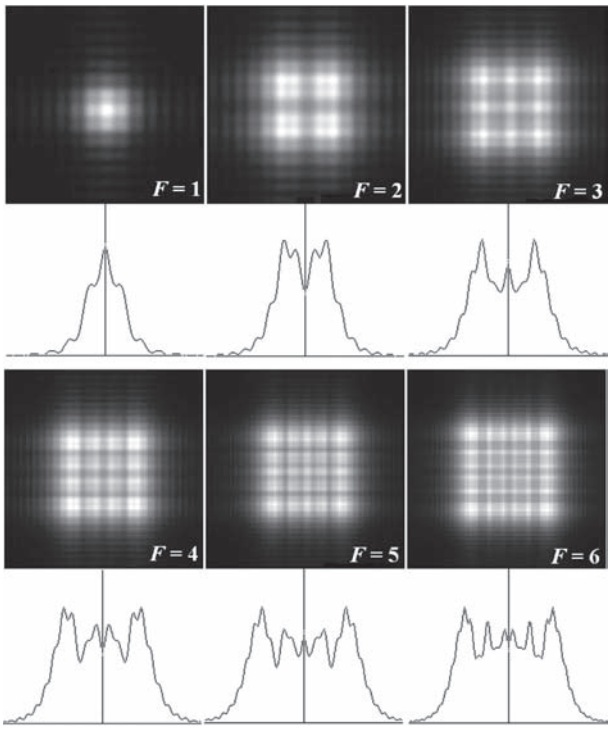

Figure 3. 2D simulated Fresnel diffraction patterns and corresponding 1D intensity profiles for Fresnel numbers 1 to 6. The relative intensities of radiation maxima and the spatial distribution can be clearly seen.[16]

110 μm (aperture S_1: a = 55 μm) and 36 μm (aperture S_2: a = 18 μm) openings, a hexagonal aperture of 55 μm (aperture H_1: a = 27.5 μm) openings and a rectangular aperture of 282 μm × 36 μm (aperture R_1: a = 18 μm) openings.

The correlation between experimentally obtained patterns with the simulated diffraction patterns is illustrated in **Figure 4** for an 81 nm thick PS film with aperture S_1. Values of F are calculated for each experiment using Equation 1. The experimental parameters l and a are chosen to produce nearly integer values of F, so that the diffraction intensity patterns are clearly resolved. For Figure 4a, the calculated F is 3.94 ± 0.07 (a = 55 μm, l = 2.16 ± 0.04 mm) while for Figure 4b it is 6.09 ± 0.17 (a = 55 μm, l = 1.40 ± 0.04 mm). In further discussions, the closest integer value of F is mentioned for the experimentally obtained structures and simulated intensity patterns.

The first column images in Figure 4 are of patterned PS film, the second column shows simulated intensity pattern corresponding to the same F, while the third column shows overlap images and correlates each intensity maxima with the pattern on the film. It is evident that relief structures form where the laser intensity is higher. Interestingly, a unit cell of the polymeric structures guided by the diffraction pattern is already about an order of magnitude smaller than the aperture size, but the line widths are even smaller.

In **Figure 5**, the effect of the film thickness on pattern formation is illustrated, keeping the optical conditions unchanged (F, i.e., a and l). Figure 5a shows the simulated intensity pattern corresponding to F = 8. For a 39 nm thick film ($L_c \approx 7$ μm, $w_c \approx 1.4$ μm), the pattern on the polymer film is comparable to the simulated image, where patterns appear corresponding to each intensity maxima (Figure 5b), separated by a distance of ≈7 μm near the center of the pattern. Therefore, patterning becomes possible on the scale which is about one order of magnitude smaller than the mask used (S_1, opening size 110 μm). With the increased film thickness of 91 nm ($L_c \approx 9.5$ μm, $w_c \approx 2.8$ μm), finer details start to disappear and only the gross pattern with a distorted interior is seen (Figure 5c). For a thicker film (135 nm; $L_c \approx 14$ μm, $w_c \approx 4$ μm), only the outer square pattern is seen, as the intensity maxima adjacent to the edge are most prominent

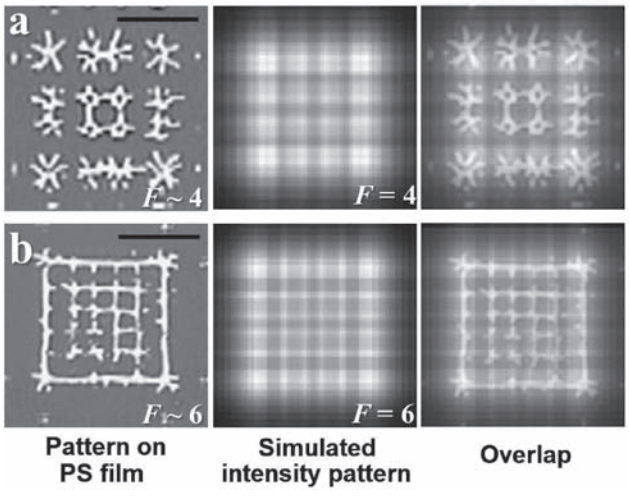

Figure 4. Comparison of the optical images of experimentally generated patterns on PS film of thickness 81 nm with the simulated images. a) Comparison for $F \approx 4$ (a: 55 μm, l: 2.16 mm); b) comparison for $F \approx 6$ (a: 55 μm, l: 1.40 mm). Overlap images in both the cases show correspondence of intensity maxima with the pattern on the film. (Scale bar: 50 μm).

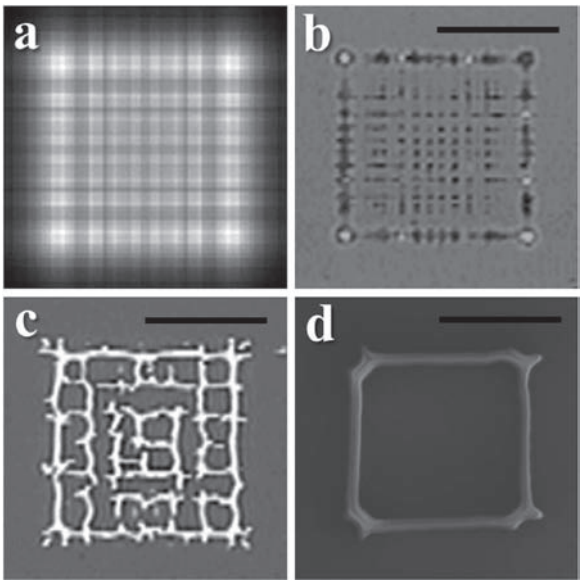

Figure 5. Comparison of patterns on PS thin films when the film thickness is varied keeping diffraction conditions constant. a) Simulated intensity distribution corresponding to F = 8. Patterns formed on PS films of thickness b) 39 nm, c) 91 nm, and d) 175 nm at $F \approx 8$ (a: 55 μm, l: 1.04 mm). (Scale bar: 50 μm)

small NANO MICRO

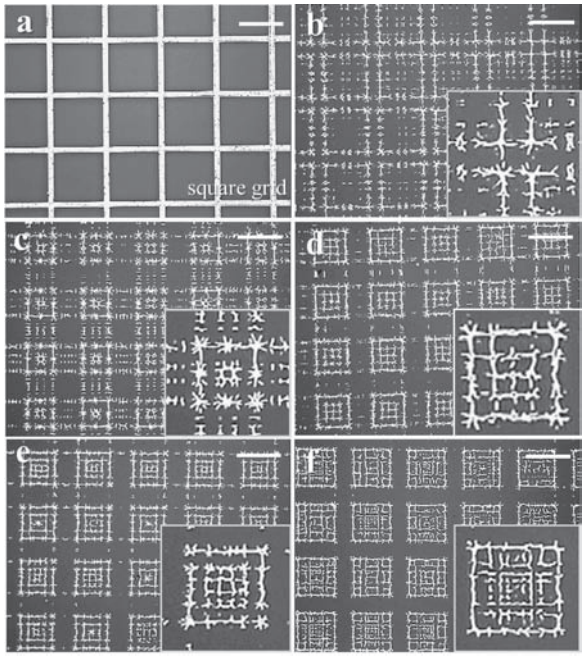

Figure 6. Comparison of patterns on PS thin films when diffraction conditions are changed, keeping the same film thickness. An optical micrograph (a) shows the square-opening transmission electron microscopy (TEM) grid used for patterning; b–f) Images correspond to a patterned PS film of thickness 81 nm and different Fresnel numbers: $F \approx 2$ (*a*: 55μm, *l*: 4.24 mm), 4 (*a*: 55μm, *l*: 2.12 mm), 5 (*a*: 55μm, *l*: 1.72 mm), 6 (*a*: 55μm, *l*: 1.4 mm) and 8 (*a*: 55μm, *l*: 1.04 mm), respectively. Insets show the enlarged unit-cell patterns formed within each aperture opening. (Scale bar: 100 μm)

(Figure 5d). The relief structures corresponding to the weaker intensity maxima completely disappear in thicker films because of the reduced energy imparted per unit volume of the film. Thus, the size of patterns formed on thin polymer films is determined by a competition between the size of the diffraction patterns and the characteristic length scales of the wrinkles (L_c and w_c) formed without any aperture.

In **Figure 6**, effect of F on the pattern formation is shown for an 81 nm thick PS film ($L_c \approx 9$ μm, $w_c \approx 2.8$ μm) using the aperture S_1 (Figure 6a). It is evident from the figure that finer features start appearing within a unit-cell pattern when the aperture is brought closer to the film, owing to the finer diffraction patterns at higher F (Figure 3). For relatively small values of F ($F \leq 4$), the diffraction patterns of neighboring cells interfere to form a more continuous pattern, which results in less distinct boundaries of unit cells. The resulting structure is a connected grid-like structure (Figure 6b,c). For higher values of F, the unit-cell pattern acquires a clear identity with a greater density of finer features within each cell. For $F \approx 8$, the interline spacing within a box is about 10 μm, which is an order of magnitude smaller than the size of opening in the aperture (110 μm) and same length scale as the diffraction pattern. The line widths of the polymer pattern are much finer (≈3 μm). The ordered pattern formation occurs only in that part of the aperture opening where the interline spacing (L_c in Figure 2) is less than the distance between the neighboring intensity maxima. For example, L_c for the 81 nm film is about 9 μm and thus ordered formation occurs for all F shown in Figure 6. In contrast, patterns in Figure 5c,d

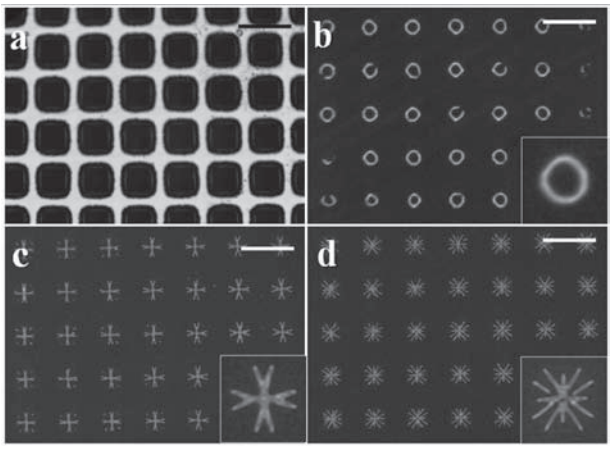

Figure 7. Optical micrographs of a) the 400 mesh square-opening TEM grid used for patterning, b) patterned PMMA film of thickness 98 nm for $F \approx 2$ (*a*: 18 μm, *l*: 0.56 mm), c) patterned PMMA film of thickness 78 nm $F < 1$ (*a*: 18 μm, *l*: 1.6 mm), and d) patterned PMMA film of thickness 78 nm $F \approx 2$ (*a*: 18 μm, *l*: 0.48 mm). (Scale bar: 50 μm)

replicate the diffraction pattern incompletely owing to the L_c of thicker films being larger than the separation between intensity maxima in the imposed diffraction pattern. Also, the gross sizes of separated unit cells vary from 65 μm (for $F \approx 5$) to 75 μm (for $F \approx 8$), which is about a 30–40% reduction from the unit-cell size on the aperture. The quality of the pattern is not so good in terms of fabrication of high fidelity structures; however, it may provide an effective and quick solution to surface texturing and low-precision structures.

Next, patterns generated by a square aperture with smaller openings (S_2, a = 18 μm) were examined on thin PMMA films. F, being a quadratic function of a, rapidly drops to lower values. Moreover, for $F \geq 3$, the separation of intensity maxima within a square aperture becomes smaller than the characteristic length scales of the thin film ($h > 75$ nm) and therefore features within the unit cell are generally absent. **Figure 7** shows the patterns formed using aperture S_2 (Figure 7a) on 78 and 98 nm thick films. On a film with thickness 98 nm ($L_c \approx 15$ μm, $w_c \approx 2.4$ μm), only one circular, ring-like pattern in each aperture opening is observed when the value of F is kept at nearly 2 (Figure 7b). The diameter of the circular pattern is ≈18.5 μm with a line width of ≈3 μm, both of which are close to the characteristic length scales of the relief patterns on 98 nm thick PMMA films (Figure 2). Furthermore, the size of the structure is approximately half that of the opening (36 μm) of the aperture used. As film thickness is decreased to 78 nm ($L_c \approx 13$ μm, $w_c \approx 2.2$ μm), finer features start appearing and the pattern becomes increasingly fragmented and multibranched with the appearance of four-fold symmetric and radially oriented features (Figure 7c,d). The overall size of the pattern in this case is about 28 μm, which is ≈22% smaller than the mask opening, with the line width of ≈2 μm. In such cases, both the ring pattern and the star pattern generated are remarkably robust and well defined over large areas. Clearly, complex patterns of this nature cannot be produced by photolithography or by any guided self-assembly-based technique without using an intricate mask or template of matching complexity.

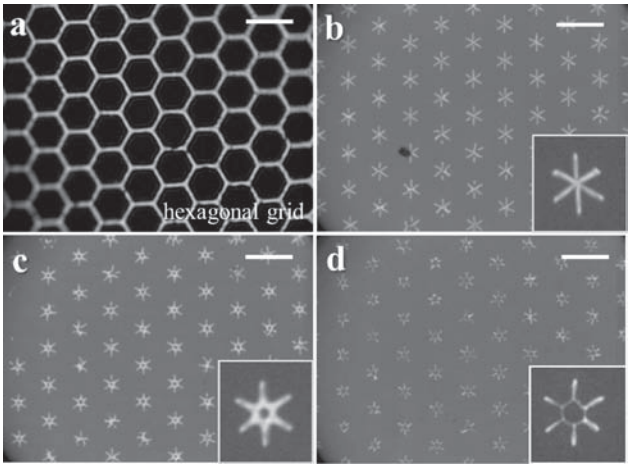

Figure 8. Optical micrographs of a) the hexagonal-opening TEM grid used for patterning, b) $F \approx 9$ (a: 27.5 μm, l: 0.24 mm), c) $F \approx 4$ (a: 27.5 μm, l: 0.52 mm), and d) $F \approx 1$ (a: 27.5 μm, l: 1.44 mm) patterned PMMA film of thickness 98 nm. (Scale bar: 100 μm)

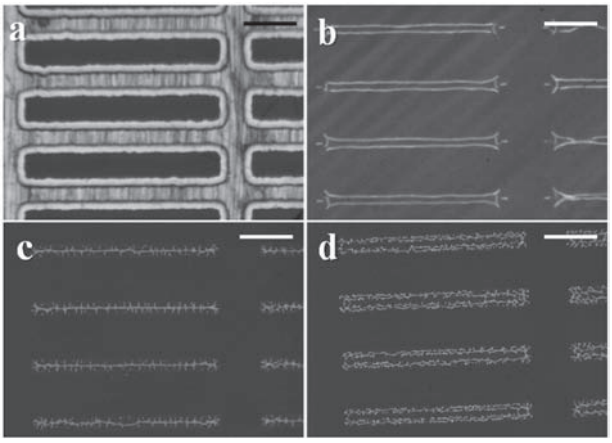

Figure 9. Optical micrographs of: a) rectangular openings of the TEM grid used as a mask, b) patterned PS film of thickness 138 nm with $F \approx 4$ (a: 18 μm, l: 0.24 mm), c) patterned PS film of thickness 75 nm with $F \approx 1$ (a: 18 μm, l: 0.8 mm), and d) patterned PS film of thickness 75 nm with $F \approx 2$ (a: 18 μm, l: 0.48 mm) (Scale bar: 50 μm)

A grid of hexagonal openings (H_1, a = 27.5 μm) produces six-fold symmetric star-shaped patterns on 98 nm thick PMMA films ($L_c \approx 15$ μm, $w_c \approx 2.4$ μm) as shown in **Figure 8**. The gross size of the unit-cell pattern is ≈36 μm (≈35% smaller than the mask opening) with a line width of ≈2 μm,. Moreover, the six-fold symmetry along with the radial alignment arises from the similar symmetry in the mask. When the aperture is moved away from the film (F decreased), a circular pocket appears at the center (images in Figure 8b–d). This may be due to the fact that for lower values of F, laser intensity is concentrated more near the center (Figure 3) and after absorption in the silicon substrate, heat diffuses radially, giving rise to the formation of a central circular ring.

Patterns depicted in Figure 7, 8 are examples of beyond-the-mask patterning, where fairly complex shapes that are not otherwise easily fabricated by other means are produced from simple masks.

The patterns created on PS films of thickness 138 and 75 nm by a rectangular aperture (R_1, **Figure 9**a) with opening dimensions of 282 μm × 36 μm are shown in Figure 9. Patterns evolved in the form of smooth 2.5 μm-thick twin lines separated by ≈12 μm (Figure 9b) on a thicker PS film (138 nm, $L_c \approx 14$ μm, $w_c \approx 4$ μm). However, for a thinner film (75 nm, $L_c \approx 8.5$ μm, $w_c \approx 2.8$ μm), patterns were fragmented (Figure 9c,d). Moreover, as F is increased from 1 (Figure 9c) to 2 (Figure 9d), splitting of the single line into two parallel lines is observed (the smaller dimension of the rectangular opening is used in the calculation of F). The width of the pattern (twin or single line) is 12–21 μm which is ≈66% smaller than the mask opening. Further the width of the fine lines bears no relation to the mask opening, but is determined only by the film thickness.

Atomic force microscope (AFM) surface topographs of these patterns confirm that they are in the form of surface relief structures with aspect ratios (height to width) of less than 1. **Figure 10**a shows a pattern consisting of square-shaped enclosures in a PS film of thickness 175 nm for $F \approx 8$. An AFM topograph of a single square shaped enclosure is shown in Figure 10b. It is evident from the height profile that

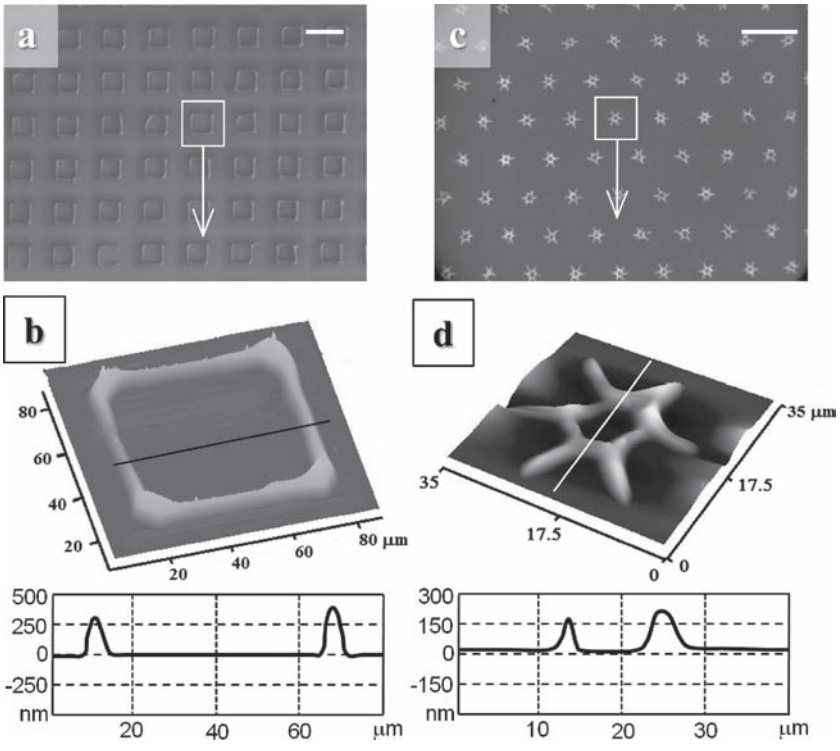

Figure 10. a) Scanning electron micrograph of a patterned PS film 175 nm thick, (a: 55 μm, l: 1.04 mm, $F \approx 8$). b) AFM topograph of a single feature highlighted in (a). c) Optical micrograph of a patterned PMMA film 95 nm thick (a: 27.5 μm, l: 0.52 mm, $F \approx 4$). d) AFM topograph of a single feature highlighted in (c). (Scale bars in (a) and (c): 100 μm)

small NANO MICRO

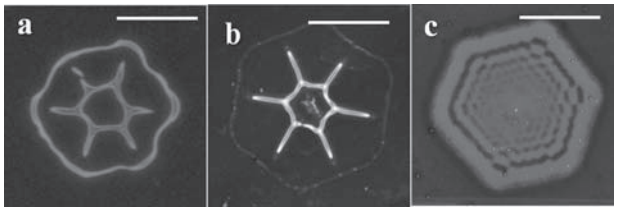

Figure 11. Patterns produced with a hexagonal aperture on a) a PS film (88 nm thick), b) a PMMA film (95 nm), and c) a PdSH film (90 nm thick) using identical optical conditions ($F \approx 9$, *a*: 27.5 μm, *l*: 0.24 mm). (Scale bar: 20 μm)

the height of these features is more than the film thickness. In this image, the protrusions are about 300 nm tall, formed on a 175 nm-thick PS film. Similarly in Figure 10c, star-shaped enclosures on a 95 nm-thick PMMA film are shown and Figure 10d shows an AFM scan of a single feature from this pattern, the height of which is about 180 nm.

In addition to the high molecular weight, nonabsorbing polymers like PS and PMMA, a smaller organo-metallic molecule, palladium hexadecylthiolate (PdSH), which absorbs 355 nm radiation, was also employed to assess the role of laser absorption in the patterning media. **Figure 11** compares the patterns generated on thin films of PS (88 nm), PMMA (95 nm), and PdSH (90 nm) using a hexagonal aperture (H_1, 55 μm opening). All the patterns were made using identical optical conditions, i.e., $F \approx 9$ (*a*: 27.5 μm, *l*: 0.24 mm). It is evident from the images that the response to the laser pulse is qualitatively the same in the case of the nonabsorbing polymers (PS and PMMA), which show only a few broad patterns. On the other hand, PdSH shows an entirely different pattern, with all the intricate features of the diffraction pattern reproduced inside. This becomes possible due to the low melt viscosity of lower-molecular-weight PdSH, which gives a faster kinetic response in the structure formation on thin films.

In closing, we make a few observations to aid any future work on further reducing the pattern dimensions using the method proposed here. In principle, one could further decrease the aperture size and aperture distance to produce smaller patterns where both L_c and w_c are in the submicrometer range. This may become possible for small molecules or low-molecular-weight polymers. Moreover, to engender near-field diffraction effects ($F > 1$) with smaller aperture widths, the laser wavelength and aperture distance should be as small as possible (Equation 1). The laser wavelength cannot be much below 200 nm (deep UV). As an example, for a 2 μm aperture opening, an aperture distance close to 1 μm is needed to achieve $F = 5$. This should be possible with nanopositioners. Another limitation on the method may however arise from the fragmentation of patterns observed for lower values of L_c with or without the use of an aperture. This loss of pattern definition may be because of the lower inertia of thinner films leading to more uncontrolled wrinkling. This aspect requires further optimization of the laser and film parameters. Smoothness of the grid edges is also necessary in the formation of sharp diffraction patterns, especially for the smaller grids.

3. Conclusion

An ultrafast, large-area micropatterning technique of thin films of nonabsorbing polymers (PS and PMMA) using a nanosecond-pulsed laser is demonstrated, which proves to be a simple, flexible, and direct method. Exposure to a single laser pulse (≈8 ns) causes absorption in the form of heat in silicon, which provides sufficient energy to the polymer film to locally melt, reorganize, and rapidly freeze to form wrinklelike surface relief structures. Characteristic length scales of relief structures formed upon laser exposure without apertures are found to increase linearly with the film thickness. Near-field diffraction effects in the patterning are incorporated by placing small periodic apertures of different sizes and geometry and are fine-tuned by changing the distance between aperture and thin film. Relief patterns on the thin films are formed by a competition between the characteristic length scales of wrinkle formation and the imposed diffraction pattern. Using a large opening aperture with large value of *F* on thinner polymer films (<50 nm), patterns an order of magnitude smaller than the mask are obtained, however, the fidelity of these structures is poor. Relatively thicker films (>90 nm) produce smooth patterns of some regular shapes such as square, circular, star-shaped patterns and open microchannels, etc., that can find application in microfluidics and biological microarrays. Further, multifold symmetric complex structures are observed in thinner films (<90 nm) with smaller apertures. Also, a size reduction of 22–66% is observed in the unit cell of the patterns formed as compared to the aperture opening. Finally, an absorbing film of PdSH is shown to produce much more complex structures, aided by its low viscosity and therefore better kinetics of the material to form these structures.

4. Experimental Section

A Nd-YAG nanosecond-pulsed laser (Quanta-Ray Lab, Spectra Physics) is employed as the coherent light source for the experiments. 355 nm radiation is used, which is the third harmonic of its fundamental wavelength (1064 nm). The fluence is varied between 100–400 mJ cm^{-2} and tuned around the onset of visible surface patterns, avoiding film rupture, which works out to be 250 mJ cm^{-2}. Unless otherwise mentioned, in all experiments only a single laser pulse (≈8 ns) of 250 mJ cm^{-2} fluence was used. All experiments were done with parallel laser beams without using any kind of lens or focusing mechanism. The experimental setup, as shown in Figure 1, consists of a periodic aperture, i.e., commercially available TEM grids, namely Gilder 200 mesh grids, Veco 400 mesh grids, Veco hexagonal 300 mesh grids, and Veco Slotted Pattern 75/300 mesh grids. Gilder 200 mesh grids have square apertures of 110 μm, Veco 400 mesh grids have square apertures of 36 μm, Veco hexagonal 300 mesh grids have 55 μm openings, while Veco Slotted Pattern 75/300 mesh grids have rectangular openings of 282 μm × 36 μm. The aperture is held using a micromanipulator to allow precise changing of the distance between aperture and substrate (precision x-y: 100 μm, z: 40 μm). PS and PMMA of average molecular weights, 280 000 and 120 000, respectively, were procured from Sigma Aldrich. Thin films ranging from

30 to 400 nm thick were spin-coated on thoroughly cleaned substrates (silicon wafer/quartz/glass) by using 0.5–5 w/v% polymer solutions in HPLC-grade toluene. PdSH, $Pd(SC_{16}H_{33})_2$ was prepared by mixing and vigorously stirring equal amounts of Pd acetate and hexadecanethiol in toluene.[17] The resulting thiolate was dried and washed with methanol and acetonitrile to remove excess thiol and then dissolved in toluene. Thin films of this material were spin-coated on cleaned substrates using this solution. Thickness measurements of thin films coated on substrates were carried out using an ellipsometer (Nanofilm, EP^3-SE). Imaging of the patterned films was done using an optical microscope (Leica DMLB 100s), a field-emission scanning electron microscope (Zeiss Supra 40VP) and an atomic force microscope (Veeco NanoMan). A java applet was used to calculate the diffraction pattern and intensity distribution for different Fresnel numbers.[16] Calculation of mean separation between wrinkle lines of random surface relief patterns generated from the exposure of polymer films with laser without any mask, was done by drawing a 6×8 grid in three different images and taking the mean value of the distance between two intersections with the standard deviation as the error bars. The line-width of these patterns was calculated by taking 10 point averages in three different images.

Acknowledgements

This work is supported by a DST IRHPA grant and Units of Nanosciences at IIT Kanpur and JNCASR Bangalore. A.V. acknowledges the initial efforts of Sruthi Murlidharan in setting up the experiments. Useful discussions regarding heat transfer calculations in silicon and polymer film with Ramki Kalyanaraman and Jeremy Strader are gratefully acknowledged.

[1] a) T. R. Hebner, C. C. Wu, D. Marcy, M. H. Lu, J. C. Sturm, *Appl. Phys. Lett.* **1998**, *72*, 519; b) Z. Nie, E. Kumacheva, *Nature Mater.* **2008**, *7*, 277.

[2] a) T. B. Cao, Q. B. Xu, A. Winkleman, G.M. Whitesides, *Small* **2005**, *1*, 1191; b) P. Greil, *Adv. Eng. Mater.* **2000**, *2*, 339.

[3] a) M. Geissler, Y. Xia, *Adv. Mater.* **2004**, *16*, 1249; b) Y. Xia, G. M. Whitesides, *Angew. Chem. Int. Ed.* **1998**, *37*, 550.

[4] a) A. M. Higgins, R. A. L. Jones, *Nature* **2000**, *404*, 476; b) A. Sehgal, V. Ferreiro, J. F. Douglas, E. J. Amis, A. Karim, *Langmuir* **2002**, *18*, 7041; c) K. Y. Suh, H. H. Lee, *Adv. Mater* **2002**, *14*, 346; d) D. Julthongpiput, W. Zhang, J. F. Douglas, A. Karim, M. J. Fasolka, *Soft Matter* **2007**, *3*, 613; e) M. Geoghegan, C. Wang, N. Rhese, R. Magerle, G. Krausch, *J. Phys: Condens. Matter* **2005**, *17*, S389; f) M. Cavallini, C. Albonetti, F. Biscarini, *Adv. Mater.* **2009**, *21*, 1043; g) B. Yoon, H. Acharya, G. Lee, H.-C. Kim, J. Huh, C. Park, *Soft Matter* **2008**, *4*, 1467; h) G. G. Baralia, C. Filiatre, B. Nysten, A. M. Jonas, *Adv. Mater.* **2007**, *19*, 4453; i) D. H. Kim, M. J. Kim, J.-Y. Park, H. H. Lee, *Adv. Funct. Mater* **2005**, *15*, 1445.

[5] a) E. Schaffer, T. Thurn-Albrecht, T. P. Russell, U. Steiner, *Nature* **2000**, *403*, 874; b) E. Schaffer, T. Thurn-Albrecht, T. P. Russell, U. Steiner, *Europhys. Lett.* **2001**, *53*, 518; c) S. Srivastava, D. Bandyopadhyay, A. Sharma, *Langmuir* **2010**, *26*, 10943; d) S. Srivastava, P. D. S. Reddy, C. Wang, D. Bandyopadhyay, A. Sharma, *J. Chem. Phys.* **2010**, *132*, 174703; e) S. Y. Chou, C. Keimel, J. Gu, *Nature* **2002**, *417*, 835; f) M. Gonuguntla, A. Sharma, S. A. Subramanian, *Macromolecules* **2006**, *39*, 3365.

[6] a) G. Reiter, *Phys. Rev. Lett.* **1992**, *68*, 75; b) G. Reiter, *Langmuir* **1993**, *9*, 1344; c) A. Sharma, G. Reiter, *J. Colloid Interf. Sci.* **1996**, *178*, 383; d) R. Xie, A. Karim, J. F. Douglas, C. C. Han, R. A. Weiss, *Phys. Rev. Lett.* **1998**, *81*, 1251; e) R. V. Craster, O. K. Matar, *Rev. Mod. Phys.* **2009**, *81*, 1131.

[7] a) J. S. Sharp, R. A. L. Jones, *Adv. Mater.* **2002**, *14*, 799; b) P. J. Yoo, K. Y. Suh, S. Y. Park, H. H. Lee, *Adv. Mater.* **2002**, *14*, 1383; c) E. P. Chan, A. J. Crosby, *Adv. Mater.* **2006**, *18*, 3238; d) A. Schweikart, A. Fery, *Microchim. Acta* **2009**, *165*, 249; e) J. Y. Chung, A. J. Nolte, C. M. Stafford, *Adv. Mater.* **2009**, *21*, 1358; f) J. S. Sharp, K. R. Thomas, M. P. Weir, *Phys. Rev. E* **2007**, *75*, 011601; g) X. He, J. Winkel, W. T. S. Huck, *Adv. Mater.* **2009**, *21*, 2083; h) J. Genzer, J. Groenewold, *Soft Matter* **2006**, *2*, 310; i) E. Cerda, L. Mahadevan, *Phys. Rev. Lett.* **2003**, *90*, 074302; j) K. Efimenko, M. Rackaitis, E. Manias, A. Vaziri, L. Mahadevan, J. Genzer, *Nat. Mater.* **2005**, *4*, 293; k) C.-C. Lin, F. Yang, S. Lee, *Langmuir* **2008**, *24*, 13627.

[8] a) R. Huang, *J. Mech. Phys. Solids* **2005**, *53*, 63; b) J. Groenewald, *Physica A* **2001**, *298*, 32; c) H. Huang, J. Y. Chung, A. J. Nolte, C. M. Stafford, *Chem. Mater.* **2007**, *19*, 6555; d) J. Y. Chung, T. Q. Chastek, M. J. Fasolka, H. W. Ro, C. M. Stafford, *ACS Nano* **2009**, *3*, 844.

[9] a) T. Lippert, J. T. Dickinson, *Chem. Rev.* **2003**, *103*, 453; b) R. Braun, R. Nowak, P. Hess, H. Oetzmann, C. Schmidt, *Appl. Surf. Sci.* **1989**, *43*, 352; c) D. Mills, K. W. Kolasinski, *J. Phys. D: Appl. Phys.* **2005**, *38*, 632; d) B. K. Nayak, M. C. Gupta, K. W. Kolasinski, *Nanotechnology* **2007**, *18*, 195302; e) N. S. Murthy, R. D. Prabhu, J. J. Martin, L. Zhou, R. L. Headrick, *J. Appl. Phys.* **2006**, *100*, 023538; f) P. E. Dyer, M. Pervolaraki, T. Lippert, *Appl. Phys. A* **2005**, *80*, 529; g) G. B. Blanchet, Yueh-Lin Loo, J. A. Rogers, F. Gao, C. R. Fincher, *Appl. Phys. Lett.* **2003**, *82*, 463; h) W. Pfleging, M. Torge, M. Bruns, V. Trouillet, A. Welle, S. Wilson, *Appl. Surf. Sci.* **2009**, *255*, 5453; i) J. Trice, C. Favazza, D. Thomas, H. Garcia, R. Kalyanaraman, R. Sureshkumar, *Phys. Rev. Lett.* **2008**, *101*, 017802.

[10] a) A. Lasagni, M. Cornejo, F. Lasgani, F. Muecklich, *Adv. Eng. Mater.* **2008**, *10*, 488; b) S. Shoji, Hong-Bo Sun, S. Kawata, *Appl. Phys. Lett.* **2003**, *83*, 608; c) T. Vijaykumar, N. S. John, G. U. Kulkarni, *Solid State Sci.* **2005**, *7*, 1475; d) M. Y. Shen, C. H. Crouch, J. E. Carey, R. Younkin, E. Mazur, M. Sheehy, C. M. Friend, *Appl. Phys. Lett.* **2003**, *82*, 1715; e) E. Haro-Poniatowski, E. Fort, J. P. Lacharme, C. Ricolleau, *Appl. Phys. Lett.* **2005**, *87*, 143103; f) S. Jeon, V. Malyarchuk, J. O. White, J. A. Rogers, *Nano Lett.* **2005**, *5*, 1351.

[11] a) P. E. Dyer, J. Mackay, C. D. Walton, *Optics Comm.* **2004**, *240*, 391; b) P. E. Dyer, S. M. Maswadi, C. D. Walton, M. Ersoz, P. D. I. Fletcher, V. N. Paunov, *Appl. Phys. A* **2003**, *77*, 391; c) J. A. Rodrigo, T. Alieva, M. L. Calvo, *Optics Express* **2009**, *17*, 4976;

[12] A. F. Lasagni, D. F. Acevedo, C. A. Barbero, F. Mucklich, *Polym. Eng. Sci.* **2008**, 48, 2367.

[13] a) T. Inagaki, E. T. Arakawa, R. N. Hamm, M. W. Williams, *Phys. Rev. B* **1977**, *15*, 3243; b) T. Li, C. Zhou, M. Jiang, *Polymer Bulletin* **1991**, *25*, 211.

[14] F. Beinhorn, J. Ihlemann, K. Luther, J. Troe, *Appl. Phys. A* **1999**, *68*, 709.

[15] a) M. Born, E. Wolf, *Principles of Optics*, 7th ed., Cambridge University Press, Cambridge**1999**, Chapter 14; b) M. A. Green, M. J. Keevers, *Prog. in Photovoltaics Res. and Appl.* **1995**, *3*, 189.

[16] N. Betancort, Fresnel Diffraction Applet inDigital Library Network for Engineering and Technology, Virginia Tech., http://www.dlnet.vt.edu/(accessed April 2010).

[17] P. J. Thomas, A. Lavanya, V. Sabareesh, G. U. Kulkarni, *Proc. Indian Acad. Sci. Chem. Sci.* **2001**, *113*, 611.

Received: October 31, 2010
Revised: December 22, 2010
Published online:

